Foam flow around an obstacle: obstacle-wall interaction[⋆]

S.J. Cox[1], B. Dollet[2], F. Graner[2]

[1] Institute of Mathematical and Physical Sciences and University of Wales Institute of Non-Newtonian Fluid Mechanics, University of Wales Aberystwyth, Ceredigion SY23 3BZ, UK, e-mail: `foams@aber.ac.uk`
[2] Spectrométrie Physique[⋆⋆], 140 rue de la Physique, BP 87, 38402 Saint Martin d'Hères Cedex, France

Abstract The flow of a two-dimensional foam around an obstacle, a version of the well-known Stokes experiment, provides a prototype experiment in which to study the transition from discrete to continuous properties of this complex fluid. The interaction between the obstacle and the walls of the channel is studied. The lift and drag forces on a circular obstacle are measured in numerical calculations using the Surface Evolver. The contributions to the total force of the film network and the bubble pressures are assessed. As the distance of the obstacle from the wall decreases, the lift force is found to increase significantly whereas the drag force does not vary greatly.

Key words Foam, Stokes experiment, Drag and Lift, Surface Evolver
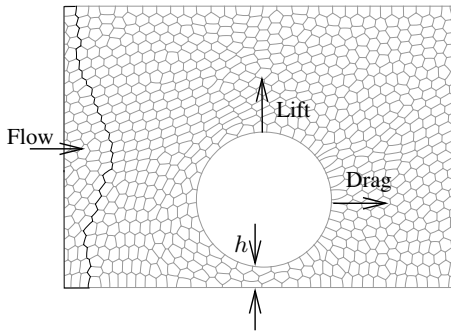
1 Introduction

Foams are found in many industrial processes and domestic applications. One of the reasons for their many uses is their complex flow properties, behaving as elastic solids at low deformation, but becoming more like an homogeneous and isotropic fluid at large deformation (Weaire and Hutzler, 1999). We wish to understand this transition, and ways to describe it, and here choose to use the familiar Stokes experiment (Stokes, 1850), originally used to measure the viscosity of a fluid through which a sphere is dropped. This classical experiment helped to establish the constitutive equation for the hydrodynamics of simple fluids; we hope to do the same for foams.

It is common to model the response of materials like foams as being shear-thinning and having a yield stress (Kraynik, 1988). With a continuum model, the problem is one of determining the extent of the yielded fluid, in addition to the drag on the obstacle (Mitsoulis, 2004). However, the yield point is not only hard to find, but is even hard to define. A foam is a convenient model to study constitutive relations, since the microscale is the scale of bubbles (not of molecules, as in most complex fluids, such as emulsions, colloids and polymer solutions), and is easily observable.

We address this question using low-velocity Stokes flow because it allows us to fix the fluid velocity, thereby eliminating the possibility of localisation of the velocity field (Debregeas *et al.*, 2001), which affects classical shear experiments. Moreover, in experiments it is then convenient to measure a force (Courty *et al.*, 2003; de Brujn, 2004; Dollet *et al.*, 2005c). This is in contrast to the *constant-force* Stokes experiments of Cox *et al.* (2000), which were plagued by intermittency in the velocity of the falling ball, due to the discrete structure of the foam.

To simplify the problem even further, we study two-dimensional (2D) foams, such as can be made by squeezing a foam between two glass plates so that the foam is one bubble thick throughout (Cox *et al.*, 2002). Then the position and shape of each bubble can be tracked over time. The sphere becomes a circular disc, around which the monolayer of bubbles is pushed within a channel of finite width. Here we study the interaction of the obstacle with the wall, partly as a prelude to the study of obstacle-obstacle interactions. Are obstacles in a foam attracted to the walls of the container, or other obstacles, or repulsed?

The energy of a 2D foam is the total length of the films. Thus the mechanism by which a foam releases energy in low-velocity flow (i.e. where viscous effects are negligible) is local neighbour-swapping rearrangements of the structure (Weaire and Hutzler, 1999). These T1 transformations are manifestations of the foam yielding, and thus supply information about the transition from elastic to plastic flow. Hence, there is energy dissipation in a foam even in the zero shear-rate limit.

Fig. 1 Foam flows from left to right around a circular obstacle. There are 750 bubbles of area $A_b = 0.16\text{cm}^2$ in a channel of width 10cm. The obstacle has diameter 4.8cm and is this case is a distance $h = 0.725\text{cm}$ from the lower wall. Drag and lift forces are measured as shown, with the convention chosen for the direction of lift being away from the wall. The foam is periodic in the horizontal direction, and the outlined region to the left is increased in area to push the foam. Note the stretching of the bubbles at the top right of the obstacle.

We quantify the response of the obstacle to the flow by measuring the lift and drag forces on it (figure 1). There are two main contributions to each of these, since, for low-velocity flow, viscous dissipation may be neglected (Dollet *et al.*, 2005b,c). These are (i) Network forces, exerted on the obstacle by the soap films attached to it, and (ii) Pressure forces, exerted by the bubbles themselves.

Our motivation in performing simulations is to understand the experimental results of Dollet *et al.* (2005b,c), in which the foam monolayer was created between a glass plate and a liquid pool. The drag forces due to the flow around a centred obstacle were expressed in terms of a yield drag, which is an extrapolation of the drag down to zero velocity. The yield drag was shown to be independent of the solution viscosity, but to decrease with increasing bubble area and to increase with increasing obstacle diameter. Further, the drag force decreases with increasing liquid fraction of the foam.

One restriction of the experiments is that only the total force (the sum of network and pressure contributions) can be measured *directly*. The network force, and possibly the pressure force, may then be estimated by subsequent image analysis. Simulations with the Surface Evolver (Brakke, 1992) allow us to measure all force components independently.

A further possibility is to use $q-$state Potts model simulations, such as those of Jiang *et al.* (1999). These are much faster than Surface Evolver simulations and therefore allow much better statistical information to be obtained, both in terms of forces and strain fields (Asipauskas *et al.*, 2003). In this Monte-Carlo method, the flow is forced by a uniform external force field on each bubble, rather than imposing a velocity. However, the restriction here is that only the network force can be measured.

The agreement of these three methods (experiment, Potts and Surface Evolver) in determining the network drag force appears to be reasonable (Dollet *et al.*, 2005d), despite having to scale the results due to differences in liquid fraction. In this paper, however, we concentrate on the Surface Evolver simulations, discussing the method in §2, the results for the off-centre obstacle in §3, and making some concluding remarks in §4.

2 Methodology

We use circular arcs to give a representation of the soap films making up the foam without discretization errors, and perform quasi-static simulations in which the foam passes through a series of equilibrium states. The value of surface tension γ is taken as one, without loss of generality.

We start the simulation from a disordered foam of 750 monodisperse bubbles which is periodic in the direction of motion. The centre of the obstacle and its radius are specified as a constraint around which the bubbles must move, in the same way as the channel walls. The boundary condition on all three constraints is that the films are free to move (slip).

T1 transformations are triggered in the relaxation of the foam when two three-fold vertices approach to within a minimal cut-off length l_c which mimics the effect of liquid fraction (Cox, 2005). The triangular geometry of the Plateau borders means that the (2D) liquid fraction is given by

$$\Phi_l = \frac{3}{2}\left(\sqrt{3} - \frac{\pi}{2}\right)\frac{l_c^2}{A_b} \approx 0.242\frac{l_c^2}{A_b} \qquad (1)$$

We choose a value of $l_c = 0.05$, corresponding to a liquid fraction of about 0.4%, i.e. a dry foam.

Once the obstacle has been shifted up or down to its desired position, the foam is relaxed to equilibrium. The quasi-static iteration procedure then commences. The foam is pushed in small steps (see figure 1) with relaxation to equilibrium at each step. We record the position of each T1 as it occurs, and the orientation of both the disappearing film and the newly formed one.

The drag and lift forces are calculated at the end of each step as the sum of pressure and network contributions. The pressure contribution is a sum over bubbles neighbouring the obstacle of the length of their shared surface multiplied by the bubble pressure. It points in the direction of the normal to the obstacle, calculated at the midpoint of the film, and is then resolved parallel (drag) and perpendicular (lift) to the direction of motion. The network contribution is the sum of the lengths of the film with one end attached to the obstacle, again resolved parallel and perpendicular to the direction of motion. In equilibrium, all films meet the obstacle at an angle of 90°, so that there is no contribution of viscous

drag. After 1500 steps, the simulations are stopped and the average saturated value of each component of force found. We also checked, in one case, that increasing the total number of bubbles in the foam does not affect the forces.

3 Results

We first demonstrate in figure 2 that the dependence of the drag force on the obstacle diameter is linear. All force values are in units which are scaled by the surface tension γ (which is taken as one in the calculations) and a length, which can be thought of as the separation between the upper and lower bounding surfaces of the foam in an experiment. (Equivalently, we could say that the force values are scaled by a line-tension $\hat{\gamma}$.)

Figure 2 also shows that increasing the bubble area at fixed channel width has only a small effect on the drag force on a centred obstacle. The cut-off length l_c is increased with increasing bubble area to keep the liquid fraction, from (1), constant. Since all liquid fractions in the simulations are small, the difference is minor (less than 10% of the total drag). Experimentally, the drag is seen to decrease for larger bubbles (Dollet *et al.*, 2005b); the discrepancy may be explained by a variation of liquid fraction in the experiments.

In what follows we use the same channel width as in the experiments of Dollet *et al.* (2005b,c), and the smallest bubble area and largest obstacle diameter used there. The channel has width 10cm and contains a circular obstacle of diameter 4.8cm. The bubble area is $A_b = 0.16\text{cm}^2$. We vary the distance of the obstacle from the wall between $h = 0.1$cm and $h = 2.6$cm (at which point the obstacle is in the centre of the channel).

The drag, lift and total forces on the obstacle are shown in figure 3 for three values of the obstacle-wall separation h. The drag forces rise over the first few hundred iterations until they saturate to a plateau value. We take this initial transient to be of duration 600 iterations throughout, although it is only really appropriate for the network drag force. Pressure forces (drag and lift) show great variability but fewer rapid fluctuations.

For different values of the separation h we fit each force trace to a constant. The result, in figure 4, shows that the network and pressure drag forces both decrease with separation. Even more strikingly, as the separation decreases, the lift force on the obstacle, pulling it away from the channel wall increases rapidly. That there is a small but finite lift in the case of a centred obstacle indicates the asymmetry introduced by the disorder in the foam.

Raufaste and Thomas (2005) have shown with the Potts model that within these trends there is a further variation of the network lift force: it appears

to show peaks at distances from the wall of one and two bubble diameters, illustrating the effect of the discrete nature of the foam on the forces on the obstacle. For our data, this can only be seen at about $h = 0.4$cm
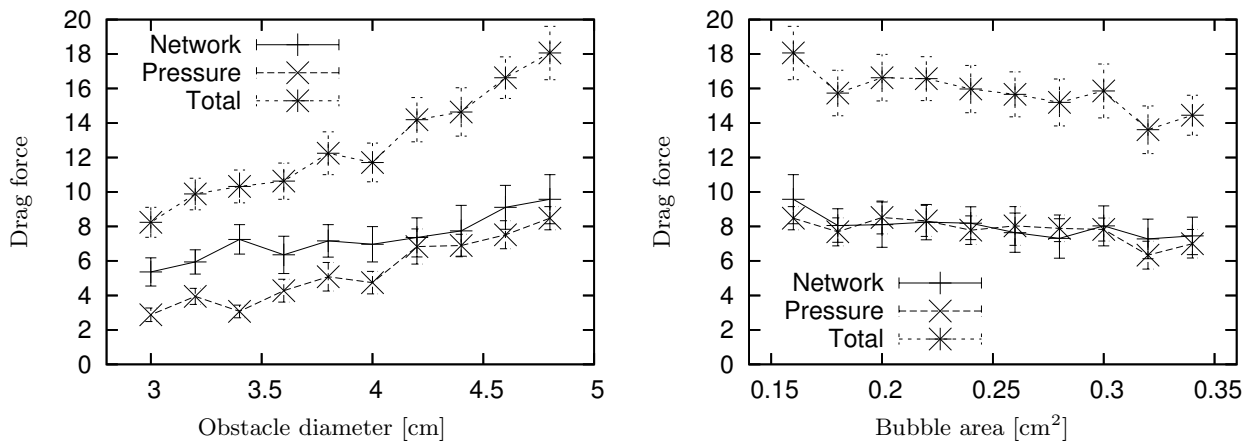
Figure 5 shows that both the network and pressure contributions to the total drag force must be taken into account. The total drag force is slightly dominated by the network over the pressure contribution, and in fact the pressure contribution appears to be almost constant as h varies. The pressure and network contributions to the lift are more scattered, but are, in general, both important.

In addition to the forces on the obstacle, we also calculate a number of fields associated with the flow, shown in figure 6. The data is binned and averaged over all iterations after the transient; 70×60 bins are used for bubble pressures and displacements, and 14×10 for the T1 field, for which there is less data. Data is shown for the same separations $h = 2.6$cm (centred case), $h = 1.35$cm amd $h = 0.1$cm, as in figure 3 (but from different simulations).

The first row of figure 6 shows the average bubble pressure. The pressure is high (black) at the left and decreases in the direction of flow (denoted x). It is symmetric for the centred obstacle, but in the off-centre case a region of high pressure is "trapped" at the bottom left of the obstacle, giving rise to the lift force.

The second and third rows of figure 6 show the averaged bubble displacements in each iteration parallel and perpendicular to the direction of motion. The displacements in the direction of flow are highest (black) between the wall and obstacle in the centred case, and lowest (white) at the stagnation points on the obstacle, as for a Newtonian fluid. For off-centre obstacles, the flow switches to the larger gap, leaving the foam below the obstacle almost stationary, even for small displacements of the obstacle from the centre-line of the channel. This is clearly seen in figure 7, which tracks the progress of a line of bubbles moving through the foam.

The vertical displacements are smaller, with black denoting upward displacements and white denoting downward ones. In the off-centre case the symmetry is broken, and the white lobe to the top right of the obstacle shows bubbles moving down behind the obstacle. This can be understood better by looking at the field of plastic events in the fourth row of figure 6. The plastic flow due to the stretching of the bubbles followed by a T1 is measured from the films which are directly involved in the T1s and represented by ellipses. This "T1 tensor" (Dollet, 2005) averages the length and direction of the line joining the centres of the two bubbles adjacent to a deleted film (dotted ellipse) and a newly created film (solid ellipse) in each of the bins. Therefore the length of the major axis of each ellipse measures the density of T1s in the box and the length of the minor axis

Fig. 2 With the bubble area fixed at 0.16cm^2, the drag force on a centred obstacle increases linearly with the diameter of the obstacle. With the obstacle diameter fixed at 4.8cm, the drag on the obstacle shows little variation with increasing bubble area. Network and pressure forces are both shown, along with their sum. The two contributions are closer for larger obstacles, but their relative size does not vary with bubble area.

measures the variability in direction of the T1s. The orientation of the dotted ellipses gives the direction in which bubbles are stretched prior to the T1.

The centred obstacle ($h = 2.6$cm) shows a symmetric situation, with bubbles being compressed in front (to the left) of the obstacle and strongly stretched behind. For an off-centre obstacle, the T1s in the wake of the obstacle move around towards the centre line of the channel. A yield-line or fracture develops in front of the obstacle down the centre of the channel, with little movement close to either wall.

4 Discussion

The drag forces on a circular obstacle increase with increasing obstacle diameter, decreasing bubble area and decreasing liquid fraction (Dollet *et al.*, 2005b). The latter dependecy can be explained because as the foam become drier, films stretch further before undergoing T1s, so that the network force on the obstacle is increased.

The simulations described here show that in explaining the origin of the drag force on an obstacle, both network and pressure contributions must be taken into account. In determining the lift, the pressure contribution would seem to be the dominant term.

We find that the drag decreases as the gap between the obstacle and the wall decreases. Roquet and Saramito (2003) show that for a Bingham fluid, often cited as a good approximation for foam, the drag varies as $h^{-9/4}$. Similarly, in 3D experiments, de Brujn (2004) found that the drag increases at small tube diameters. This marks the extent of the yielded region around a moving sphere, which he found to extend to about one sphere radius.

For a non-circular obstacle such as an aerofoil, the lift is in the opposite direction to that expected for a Newtonian fluid (Dollet *et al.*, 2005a), as for

other complex fluids (Wang and Joseph, 2004). This is usually attributed to the elasticity of the fluid. We find that, in these inviscid calculations, the lift force is repulsive, pushing the obstacle away from the walls of the channel, in contrast to the (ideal) Newtonian case.
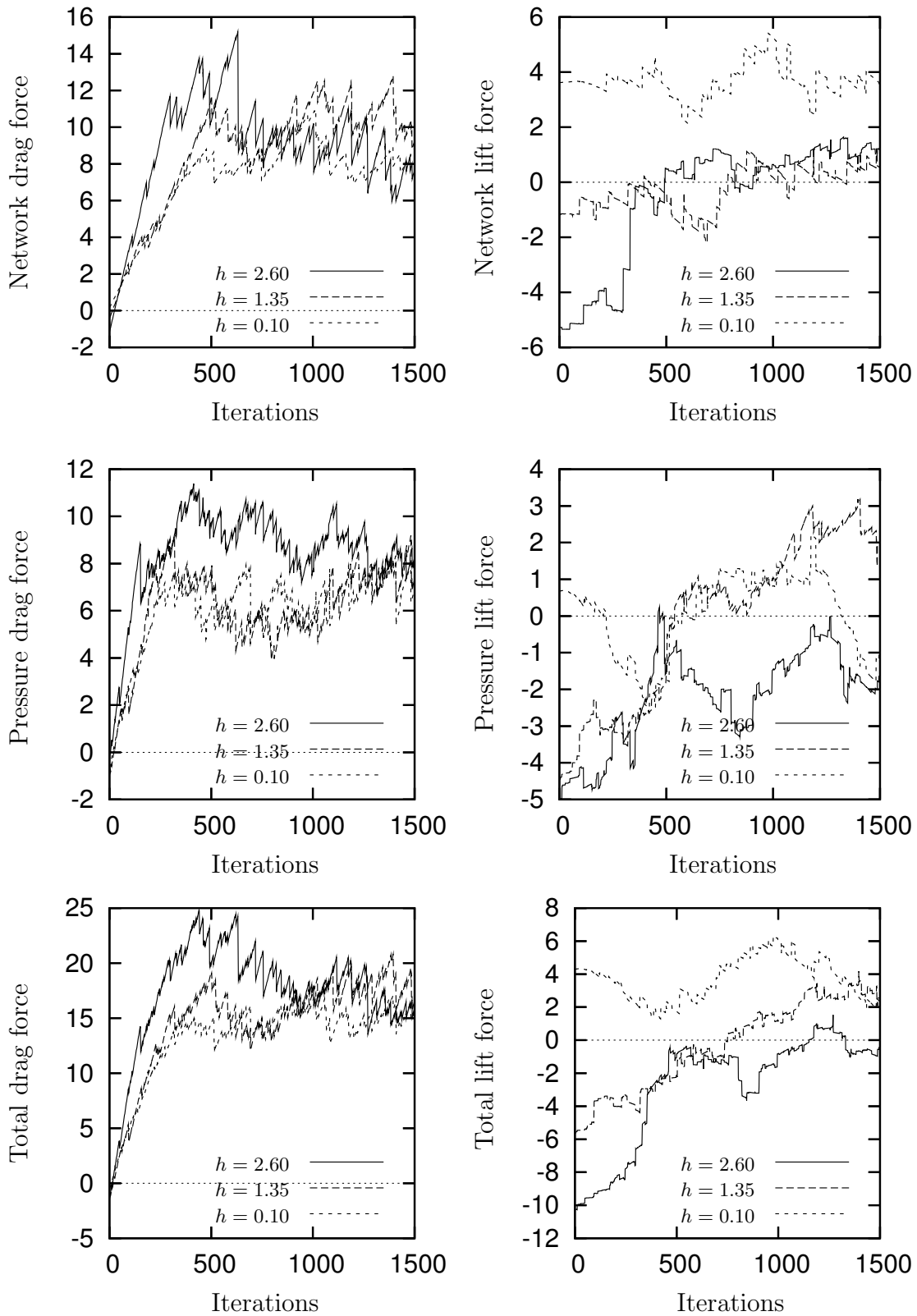
In the future we intend to simulate foam flow around non-symmetric obstacles, even in the centred case, to probe further the different contributions to drag and lift and their relation to experimental data.
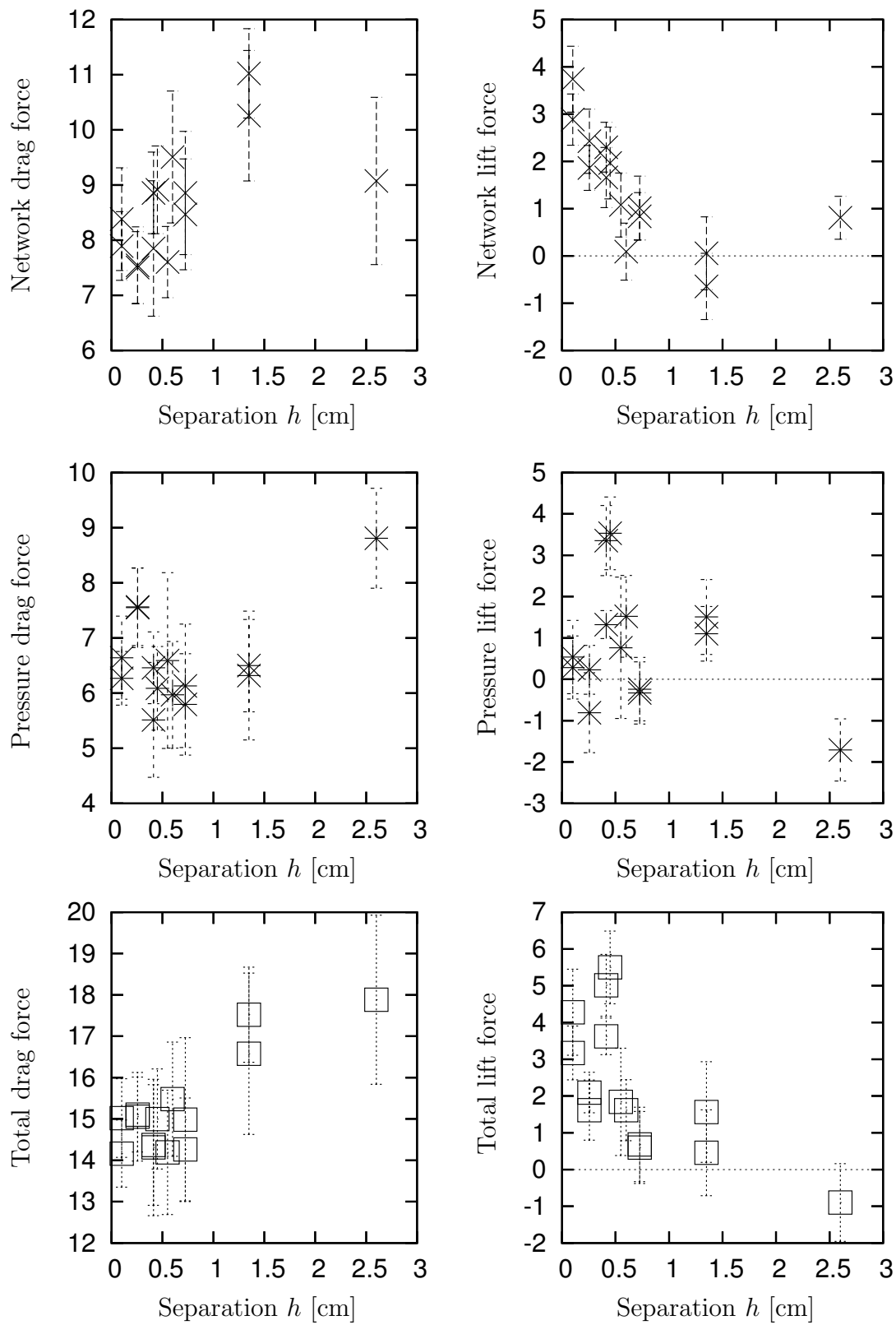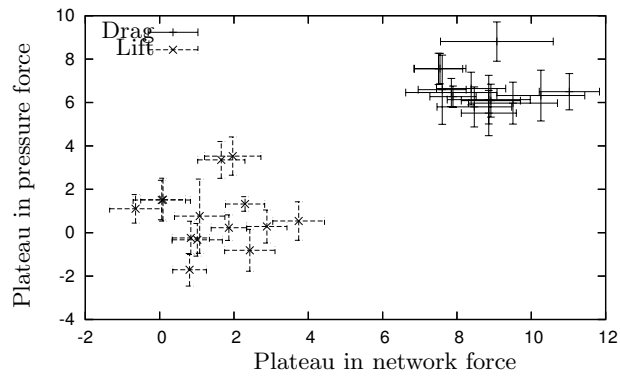
References

Asipauskas, M., Aubouy, M., Glazier, J.A., Graner, F. and Jiang, Y. 2003. A texture tensor to quantify deformations: the example of two-dimensional flowing foams. *Granular Matter* **5**:71–74.

Brakke, K. 1992. The Surface Evolver. *Exp. Math.* **1**:141–165.

de Brujn, J.R. 2004. Transient and steady-state drag in foam. *Rheol. Acta* **44**:150–159.

Courty, S., Dollet, B., Elias, F., Heinig, P. and Graner, F. 2003. Two-dimensional shear modulus of a Langmuir foam. *Europhys. Lett.* **64**:709–715.

Cox, S.J. 2005. The mixing of bubbles in two-dimensional foams under extensional shear. Submitted for publication.

Cox, S.J., Alonso, M.D., Hutzler, S. and Weaire, D. 2000. The stokes experiment in a foam. In P. Zitha, J. Banhart and G. Verbist, (eds), *Foams, emulsions and their applications.* MIT-Verlag, Bremen pp. 282–289.
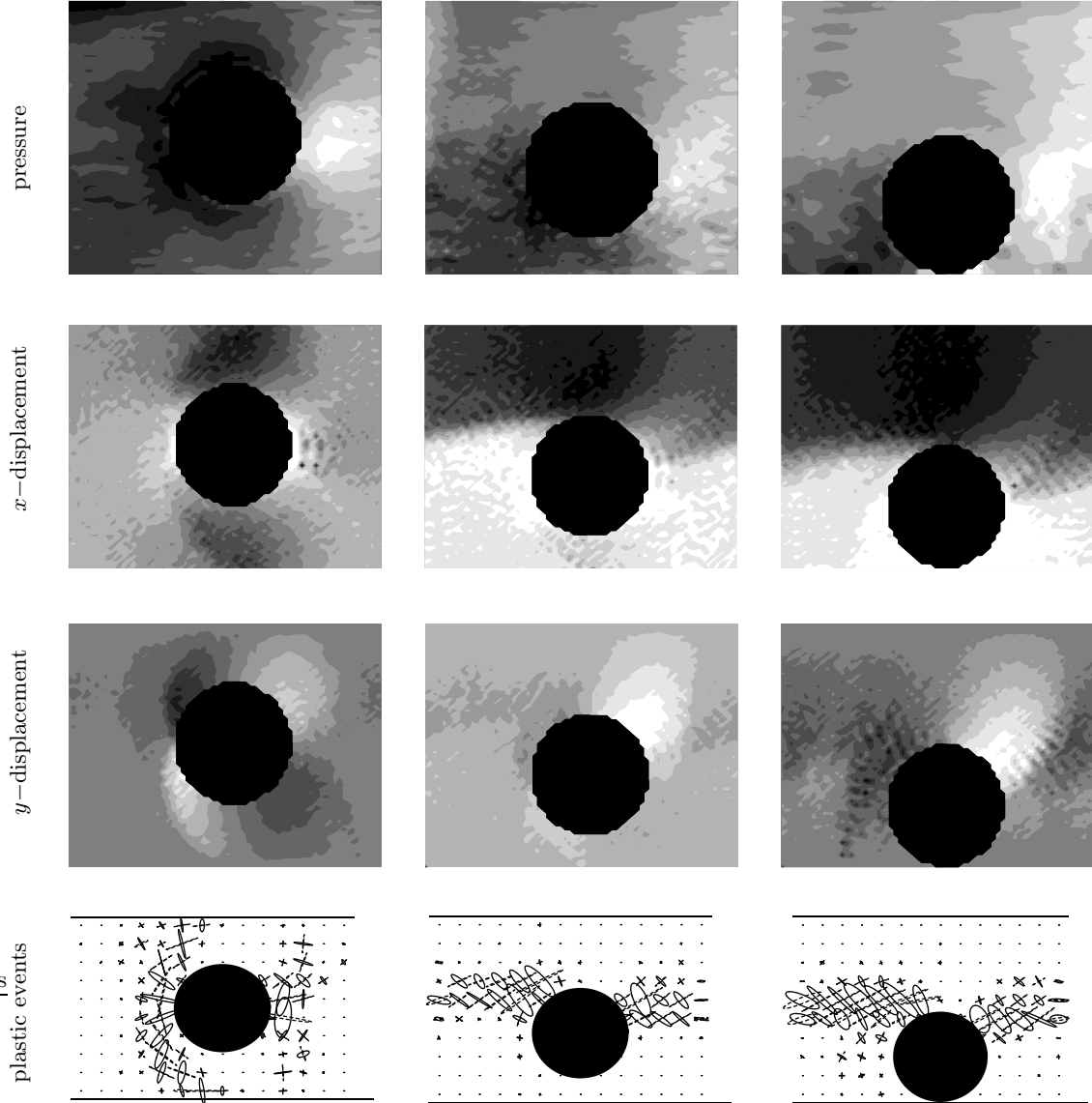
Fig. 3 The evolution of the drag and lift forces over time in three cases, including a centred obstacle ($h = 2.6$cm) and one very close to the wall ($h = 0.1$cm). There is a transient of about 600 iterations in the network contribution to the drag; this is less for the pressure contribution, but in fitting the force data to find the plateaux, we ignore all data for less than 600 iterations. Note also the large variability in the pressure lift force. The plateau values are compared in figure 4.
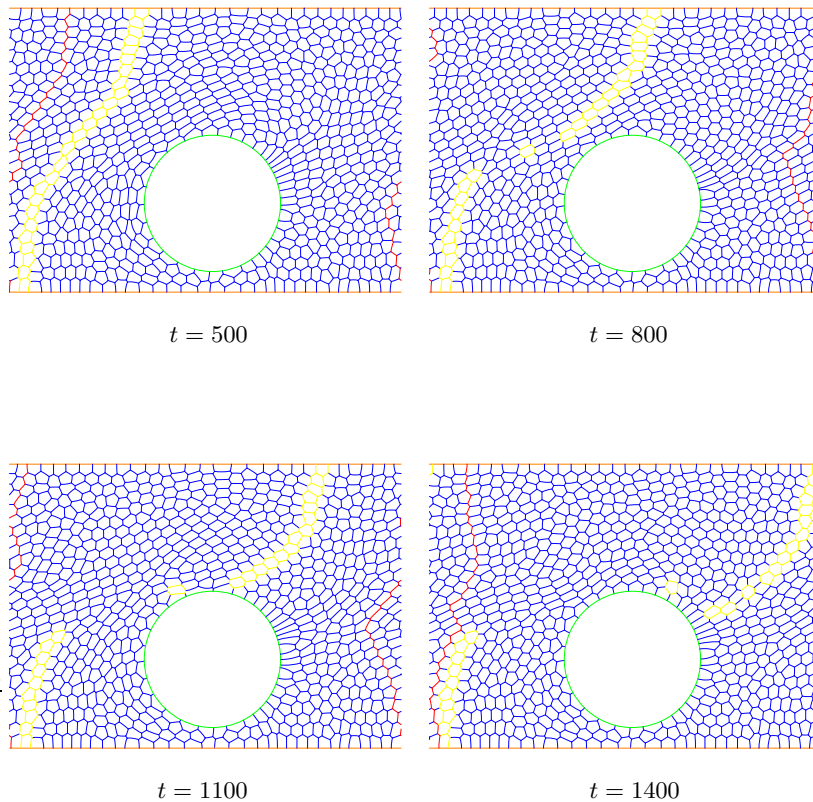
Fig. 4 The saturated (plateaux) values of the drag and lift forces as the separation h of the obstacle from the wall is varied. Note the different scales on the force axes. As the obstacle approaches the wall, the drag forces decrease slightly, and the lift forces increase significantly.

Fig. 5 The network drag force is about 20% greater than the pressure contribution to the total drag, and the data is closely clustered. Moreover, the contribution of the pressure term appears to be fairly constant. There is greater variability in the values for lift, particularly for the pressure contribution.

Fig. 6 Contour plots of relevant fields for separations of (from left to right) $h = 2.6$cm (centred), $h = 1.35$cm and $h = 0.1$cm. The data for pressure, $x-$displacement (direction of motion), y-displacement, and T1s is shown, after averaging over 900 iterations (after the transient). See text for details.

Fig. 7 Four stages in the flow of foam past an obstacle a distance $h = 0.725$cm from the wall at different iterations t. The line of light-coloured bubbles across the channel shows how the foam flows over the obstacle, with little bubble motion close to the lower wall.

Cox, S.J., Weaire, D. and Vaz, M.F. 2002. The transition from two-dimensional to three-dimensional foam structures. *Eur. Phys. J. E* **7**:311–315.

Debregeas, G., Tabuteau, H. and di Meglio, J.M. 2001. Deformation and flow of a two-dimensional foam under continuous shear. *Phys. Rev. Lett.* **87**: 178305.

Dollet, B. 2005 *Ecoulement bidimensionnel de mousses autour d'obstacles.* PhD thesis. Univ. Grenoble.

Dollet, B., Aubouy, M. and Graner, F. 2005a. Inverse Lift: a signature of the elasticity of complex fluids. Submitted for publication.

Dollet, B., Elias, F., Quilliet, C., Huillier, A., Aubouy, M. and Graner, F. 2005b. Two-dimensional flows of foam: drag exerted on circular obstacles and dissipation. *Coll. Surf. A* **263**: 101–110.

Dollet, B., Elias, F., Quilliet, C., Raufaste, C., Aubouy, M. and Graner, F. 2005c. Two-dimensional flow of foam around an obstacle: Force measurements. *Phys. Rev. E* **71**:031403.

Dollet, B., Raufaste, C., Jiang, Y., Graner, F. and Cox, S.J. 2005d. Determination of yield drag in a foam: simulations of a two-dimensional flow around a circular obstacle as a function of liquid fraction. In preparation.

Jiang, Y., Swart, P.J., Saxena, A., Asipauskas, M. and Glazier, J.A. 1999. Hysteresis and Avalanches in two-dimensional foam rheology simulations. *Phys. Rev. E* **59**:5819–5832.

Kraynik, A.M. 1988. Foam flows. *Ann. Rev. Fluid Mech.* **20**:325–357.

Mitsoulis, E. 2004. On creeping drag flow of a viscoplastic fluid past a circular cylinder: wall effects. *Chem. Eng. Sci.* **59**:789–800.

Raufaste, C. and Thomas, S. 2005. Private Communication.

Roquet, N. and Saramito, P. 2003. An adaptive finite element method for Bingham flows around a cylinder. *Comput. Meth. Appl. Mech. Eng.* **192**: 3317–3341.

Stokes, G.G. 1850. On the Effect of the Internal Friction of Fluids on the Motion of Pendulums. *Trans. Camb. Phil. Soc.* **IX**:8–149.

Wang, J. and Joseph, D.D. 2004. Potential flow of a second-order fluid over a sphere or an ellipse. *J. Fl. Mech.* **511**:201–215.

Weaire, D. and Hutzler, S. 1999. *The Physics of Foams.* Clarendon Press, Oxford.